ReaxFF: A Reactive Force Field for Hydrocarbons

Adri C. T. van Duin,[†,‖] **Siddharth Dasgupta,**[‡] **Francois Lorant,**[§] **and William A. Goddard III*,**[‡]

Department of Fossil Fuels and Environmental Geochemistry, Drummond Building, University of Newcastle, Newcastle upon Tyne NE1 7RU, United Kingdom, Materials and Process Simulation Center, Beckman Institute (139-74), Division of Chemistry and Chemical Engineering, California Institute of Technology, Pasadena, California 91125, and Institut Français du Pètrole, Geology and Geochemistry Research Division, 1-4 Avenue de Bois-Preau, 92852 Rueil-Malmaison, France

To make practical the molecular dynamics simulation of large scale reactive chemical systems (1000s of atoms), we developed ReaxFF, a force field for reactive systems. ReaxFF uses a general relationship between bond distance and bond order on one hand and between bond order and bond energy on the other hand that leads to proper dissociation of bonds to separated atoms. Other valence terms present in the force field (angle and torsion) are defined in terms of the same bond orders so that all these terms go to zero smoothly as bonds break. In addition, ReaxFF has Coulomb and Morse (van der Waals) potentials to describe nonbond interactions between all atoms (no exclusions). These nonbond interactions are shielded at short range so that the Coulomb and van der Waals interactions become constant as $R_{ij} \rightarrow 0$. We report here the ReaxFF for hydrocarbons. The parameters were derived from quantum chemical calculations on bond dissociation and reactions of small molecules plus heat of formation and geometry data for a number of stable hydrocarbon compounds. We find that the ReaxFF provides a good description of these data. Generally, the results are of an accuracy similar or better than PM3, while ReaxFF is about 100 times faster. In turn, the PM3 is about 100 times faster than the QC calculations. Thus, with ReaxFF we hope to be able to study complex reactions in hydrocarbons.

1. Introduction

The accuracy and speed of modern quantum chemistry (QC) methods allow the geometries, energies, and vibrational energies to be predicted quite accurately for small molecules. However, QC is not yet practical for studying the dynamic properties of larger molecules and solids. Consequently, it is useful to have accurate force fields (FF) to quickly evaluate the forces and other dynamical properties such as the effects of mechanical shock waves or diffusion of small molecules in polymer and mesoporous zeolites. Indeed, for hydrocarbons a number of FF, particularly MM3,[1−3] provide accurate predictions of geometries, conformational energy differences, and heats of formation. Generic FF such as DREIDING[4] and UFF[5] allow predictions for broad classes of compounds, particularly when coupled to charge equilibration[6] (*Q*Eq) or other methods for predicting charges. However, in general, these force fields do not describe chemical reactivity. An exception is the Brenner potential,[7] which leads to accurate geometries for ground states of hydrocarbons, but is formulated in such a way that it can describe bond breaking. Unfortunately, the Brenner formalism does not include the van der Waals and Coulomb interactions that are very important in predicting the structures and properties of many systems. In addition, the actual potential curves for bond breaking and reactions are often quite poorly described with the Brenner potential. Generalizations of the Brenner FF have included such nonbonded forces,[8] but without repairing

the fundamental problems in the shapes of the dissociation and reactive potential curves.

Two other bond-order-dependent force field methods are noteworthy. The Bond Energy Bond Order (BEBO) method was proposed by Johnston[9,10] based on Pauling's relation between bond length and bond order.[11] The fundamental assumption behind this method is that the path of lowest energy on going from reactant to product is one that conserves total bond order. Originally used for the H + H_2 reaction surface, it is a very good approximation to more complicated empirical forms such as LEPS surface.[12−13] While it has recently been extended to more complex reactions,[14−15] it remains mainly useful for H atom transfer reactions in a linear collision geometry.

The VALBOND method formulated by Landis and colleagues is based on the strength functions of hybrid orbitals. The motivation comes from the need to fit large distortions in the softer angle terms of valence force fields, as well as describing multiple equilibrium angles in transition metal complexes (e.g., the 90° and 180° angles in square planar complexes). Assuming that different ligand atoms, lone pairs, and radical electrons have implicit preference for p-character, VALBOND uses Lewis structure-based allocations to assign hybridizations and the geometries are obtained by minimizing defects in the hybrid orbitals. For a simple force field, it does remarkably well on structures and vibrational frequencies for a wide range of small molecules and transition metal complexes.[16−18] These methods, however, do not fully address the need to have full chemistry of the breaking and forming bonds, in addition to a proper description of the fully bonded equilibrium geometry of complex molecules.

In this paper, we develop a general bond-order-dependent potential in which the van der Waals and Coulomb forces are

---

* Author to whom correspondence should be addressed. E-mail: wag@wag.caltech.edu.
† University of Newcastle.
‡ California Institute of Technology.
§ Institut Français du Pètrole, Geology and Geochemistry Research Division.
‖ E-mail: A.C.T.van-Duin@ncl.ac.uk.

ReaxFF: A Reactive Force Field for Hydrocarbons

J. Phys. Chem. A, Vol. 105, No. 41, 2001 **9397**

TABLE 1: General Parameters

parameter	value	description	equation
λ_1	50.0	overcoordination bond order correction	3c
λ_2	15.61	overcoordination bond order correction	3d
λ_3	5.02	1−3 bond order correction	3e,f
λ_4	18.32	1−3 bond order correction	3e,f
λ_5	8.32	1−3 bond order correction	3e,f
λ_6	−8.90	overcoordination energy	6
λ_7	1.94	undercoordination energy	7a
λ_8	−3.47	undercoordination energy	7a
λ_9	5.79	undercoordination energy	7b
λ_{10}	12.38	undercoordination energy	7b
λ_{11}	1.49	valence angle energy	8b
λ_{12}	1.28	valence angle energy	8b
λ_{13}	6.30	valence angle energy	8c
λ_{14}	2.72	valence angle energy	8c
λ_{15}	33.87	valence angle energy	8c
λ_{16}	6.70	valence angle energy	8d
λ_{17}	1.06	valence angle energy	8d
λ_{18}	2.04	valence angle energy	8d
λ_{19}	36.0	penalty energy	9a
λ_{20}	7.98	penalty energy	9a
λ_{21}	0.40	penalty energy	9b
λ_{22}	4.00	penalty energy	9b
λ_{23}	3.17	torsion energy	10b
λ_{24}	10.00	torsion energy	10c
λ_{25}	0.90	torsion energy	10c
λ_{26}	−1.14	conjugation energy	11a
λ_{27}	2.17	conjugation energy	11b
λ_{28}	1.69	van der Waals energy	12b

included from the beginning and the dissociation and reaction curves are derived from QC calculations. In spirit it is derived from the central force concept used earlier by spectroscopists[19] but abandoned because a single harmonic potential between all atom pairs was inadequate for complex molecules. We have kept the central force formalism, where all atom pairs have nonbonded interactions, because it dissociates smoothly, but add local perturbations (bond, angle, torsion, etc.) to describe the complex molecules more accurately. We have attempted to obtain accurate descriptions of quantum phenomena such as resonance, unsaturated valences in radical systems, and chemical reactions. While the current work is restricted to hydrocarbons this approach is easily extended to any molecular system of any class of compounds. In a future paper we will report on our extension to CHNO-systems. Section 2 describes the general form of the reactive force field (denoted ReaxFF) and the procedure for optimizing the parameters. Section 3 presents the results for a number of systems. Section 4 discusses these results, and Section 5 presents the conclusions.

2. Force Field

Similar to empirical nonreactive force fields, the reactive force field divides the system energy up into various partial energy contributions, as demonstrated by eq 1.

$$E_{system} = E_{bond} + E_{over} + E_{under} + E_{val} + E_{pen} + E_{tors} + E_{conj} + E_{vdWaals} + E_{Coulomb} \quad (1)$$

The potential energy functions associated with each of these partial energy contributions are described below. Tables 1−6 list the parameters used in these potential functions.
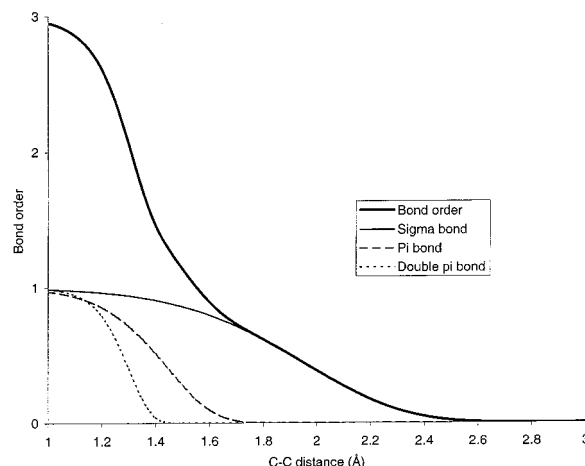

Figure 1. Interatomic distance dependency of the carbon−carbon bond order.

2.1. Bond Order and Bond Energy. A fundamental assumption of ReaxFF is that the bond order BO'_{ij} between a pair of atoms can be obtained directly from the interatomic distance r_{ij} as given in eq 2 and plotted in Figure 1. Equation 2 consists of three exponential terms: (1) the sigma bond ($p_{bo,1}$ and $p_{bo,2}$) which is unity below ∼1.5 Å but negligible above ∼2.5 Å; (2) the first pi bond ($p_{b0,3}$ and $p_{b0,4}$) which is unity below ∼1.2 Å and negligible above ∼1.75 Å, and (3) the second pi bond ($p_{bo.5}$ and $p_{bo,6}$) which is unity below ∼1.0 Å and negligible above ∼1.4 Å.

This leads to a carbon−carbon bond with a maximum bond order of 3. For carbon−hydrogen and hydrogen−hydrogen bonds, only the sigma-bond contribution is considered, leading to a maximum bond order of 1

$$BO'_{ij} = \exp\left[p_{bo,1} \cdot \left(\frac{r_{ij}}{r_o}\right)^{p_{bo,2}}\right] + \exp\left[p_{bo,3} \cdot \left(\frac{r_{ij}^{\pi}}{r_o}\right)^{p_{bo,4}}\right] + \exp\left[p_{bo,5} \cdot \left(\frac{r_{ij}^{\pi\pi}}{r_o}\right)^{p_{bo,6}}\right] \quad (2)$$

The bond orders BO'_{ij} are corrected for overcoordination and for residual 1−3 bond orders in valence angles using the scheme described in eqs 3a−f. While the 1−3 bond order correction, described in eqs 3e and 3f, is applied to all the bonds in the molecule, the overcoordination correction (eqs 3b−d) is only applied to bonds containing two carbon atoms. The final bond orders in the molecule are obtained by multiplying the bond orders from Equation 2 by the correction factors from eq 3. Figure 2 shows the effects of eqs 3a−f on the bond orders in an ethane molecule in which the C−C bond length is reduced from its equilibrium values of about 1.53 Å to 1.0 Å. This creates overcoordination on both the carbon and the hydrogen atoms, as the sum of bond orders around all atoms exceeds their valences (4 for carbon and 1 for hydrogen). As Figure (2) shows, application of Equations (3a−f) removes all of the 1−3 bond orders, correcting the overcoordination on the hydrogen atoms, and, in addition, corrects most of the additional overcoordination

TABLE 2: Atom Parameters As Used in Equations 2, 6, 7, 12, 13, and 14[a]

	bond radii			under/over coordination		Coulomb parameters			heat increments
units	r_o Å	$r_{o,\pi}$ Å	$r_{o,\pi\pi}$ Å	p_{over} kcal/mol	p_{under} kcal/mol	η EV	χ EV	γ Å	I kcal/mol
C	1.399	1.266	1.236	52.2	29.4	7.41	4.12	0.69	218.6
H	0.656	-		117.5		9.14	2.26	0.37	54.3

[a] $r_o(ij) = {}^1/_2[r_o(i) + r_o(j)]$.

TABLE 3: van der Waals Parameters Used in Equation 12[a]

atom units	r_{vdW} Å	ϵ kcal/mol	α	γ_w Å
C	3.912	0.0862	10.71	1.41
H	3.649	0.0194	10.06	5.36

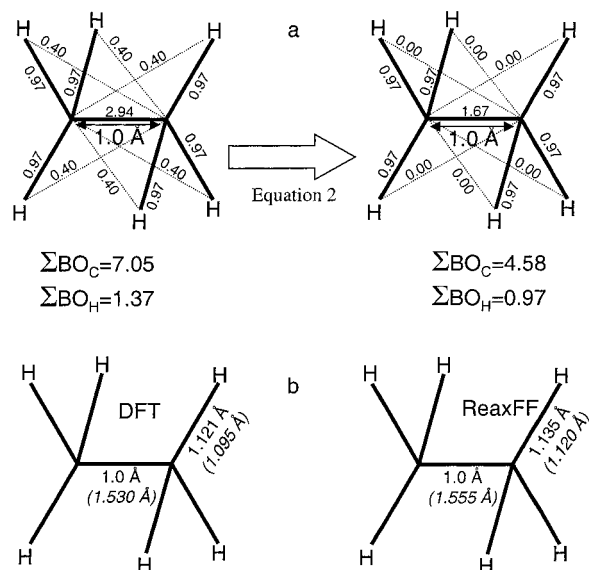[a] Arithmetic combination rules are used for all van der Waals parameters.

Figure 2. (a) Effect of the bond order correction in eq 2 on the C−C and C−H bond orders in an ethane molecule in which the C−C bond is shortened to 1.0 Å with the rest of the geometry fixed. (b) Effects of shortening of the C−C bond length in ethane to 1.0 Å on the relaxed C−H bond lengths as calculated by DFT and ReaxFF. Equilibrium C−C and C−H bond lengths are in italics and brackets.

on the carbon atoms.

$$BO_{ij} = BO'_{ij} \cdot f_1(\Delta'_i, \Delta'_j) \cdot f_4(\Delta'_i, BO'_{ij}) \cdot f_5(\Delta'_j, BO'_{ij}) \quad (3a)$$

$$f_1(\Delta_i, \Delta_j) = \frac{1}{2} \cdot \left(\frac{Val_i + f_2(\Delta'_i, \Delta'_j)}{Val_i + f_2(\Delta'_i, \Delta'_j) + f_3(\Delta'_i, \Delta'_j)} + \right.$$

$$\left. \frac{Val_j + f_2(\Delta'_i, \Delta'_j)}{Val_j + f_2(\Delta'_i, \Delta'_j) + f_3(\Delta'_i, \Delta'_j)} \right) \quad (3b)$$

$$f_2(\Delta'_i, \Delta'_j) = \exp(-\lambda_1 \cdot \Delta'_i) + \exp(-\lambda_1 \cdot \Delta'_j) \quad (3c)$$

$$f_3(\Delta'_i, \Delta'_j) = \frac{1}{\lambda_2} \cdot \ln\left\{ \frac{1}{2} \cdot [\exp(-\lambda_2 \cdot \Delta'_i) + \exp(-\lambda_2 \cdot \Delta'_j)] \right\} \quad (3d)$$

$$f_4(\Delta'_i, BO'_{ij}) = \frac{1}{1 + \exp(-\lambda_3 \cdot (\lambda_4 \cdot BO'_{ij} \cdot BO'_{ij} - \Delta'_i) + \lambda_5)} \quad (3e)$$

$$f_5(\Delta'_j, BO'_{ij}) = \frac{1}{1 + \exp(-\lambda_3 \cdot (\lambda_4 \cdot BO'_{ij} \cdot BO'_{ij} - \Delta'_j) + \lambda_5)} \quad (3f)$$

Val_i in eqs 3a−3f is the valency of atom i ($Val_i = 4$ for carbon, $Val_i = 1$ for hydrogen). Δ'_i is the degree of deviation of the sum of the uncorrected bond orders around an atomic center

from its valency Val_i, as described in eq 4.

$$\Delta'_i = \sum_{j=1}^{nbond} BO'_{ij} - Val_i \quad (4)$$

Equation 5 is used to calculate the bond energies from the corrected bond order BO_{ij}.

$$E_{bond} = -D_e \cdot BO_{ij} \cdot \exp[p_{be,1}(1 - BO_{ij}^{p_{be,1}})] \quad (5)$$

2.2. Atom Under-/Overcoordination. From the valence theory of bonding we know that the total bond order of C should not exceed 4 and that of H should not exceed 1, except in hypervalent cases. However, as Figure 2 shows, even after correction of the original bond orders BO'_{ij} a degree of overcoordination may remain in the molecule. To handle this we have added an overcoordination penalty term to the force field.

2.2.1. Over-Coordination. For an overcoordinated atom ($\Delta_i > 0$), eq 6 imposes an energy penalty on the system. The form of eq 6, ensures that E_{over} will quickly vanish to zero for under-coordinated systems ($\Delta_i < 0$). Δ_i is calculated using eq 4, using the corrected bond orders BO_{ij} from eq 3 instead of the uncorrected bond orders from eq 2.

$$E_{over} = p_{over} \cdot \Delta_i \cdot \left(\frac{1}{1 + \exp(\lambda_6 \cdot \Delta_i)} \right) \quad (6)$$

2.2.2. Under-Coordination. For an under-coordinated atom ($\Delta_i < 0$), we want to take into account the energy contribution for the resonance of the π-electron between attached under-coordinated atomic centers. This is done by eqs 7a,b where E_{under} is only important if the bonds between under-coordinated atom i and its under-coordinated neighbors j partly have π-bond character ($BO_{ij,\pi} > 0$ as calculated from the last two terms of eq 2).

$$E_{under} = -p_{under} \cdot \frac{1 - \exp(\lambda_7 \cdot \Delta_i)}{1 + \exp(-\lambda_8 \cdot \Delta_i)} \cdot f_6(BO_{ij,\pi}, \Delta_j) \quad (7a)$$

$$f_6(BO_{ij,\pi}, \Delta_j) = \frac{1}{1 + \lambda_9 \cdot \exp\left(\lambda_{10} \cdot \sum_{j=1}^{neighbors(i)} \Delta_j \cdot BO_{ij,\pi}\right)} \quad (7b)$$

2.3. Valence Angle Terms. Just as for bond terms, it is important that the energy contribution from valence angle terms goes to zero as the bond orders in the valence angle goes to zero. Equations 8a−d are used to calculate the valence angle energy contribution. We use the bond-order-dependent form in eq 8a to calculate energy associated with deviations in valence angle Θ_{ijk} from its equilibrium value Θ_o. The $f_7(BO)$ term as described in eq 8b ensures that the valence angle energy contribution disappears smoothly during bond dissociation. Equation 8c deals with the effects of over/undercoordination in central atom j on the valence angle energy. The equilibrium angle Θ_o for Θ_{ijk} depends on the sum of π-bond orders (SBO) around the central atom j as described in eq 8d. Thus, the

TABLE 4: Bond Parameters (D_e in kcal/mol) As Used in Equations 2 and 3

bond	D_e	$p_{be,1}$	$p_{be,2}$	$p_{bo,1}$	$p_{bo,2}$	$p_{bo,3}$	$p_{bo,4}$	$p_{bo,5}$	$p_{bo,6}$
C−C	145.2	0.318	0.65	−0.097	6.38	−0.26	9.37	−0.391	16.87
C−H	183.8	−0.454	12.80	−0.013	7.65				
H−H	168.4	−0.310	10.25	−0.016	5.98				

ReaxFF: A Reactive Force Field for Hydrocarbons

J. Phys. Chem. A, Vol. 105, No. 41, 2001 **9399**

TABLE 5: Valence Angle Parameters As Used in Equations 8a−d

valence angle units	$\Theta_{o,o}$ degree	k_a kcal/mol	k_b (1/radian)^2	$p_{v,1}$	$p_{v,2}$
C−C−C	71.31[a]	35.4	1.37	0.01	0.77
C−C−H	71.56	29.65	5.29		
H−C−H	69.94	17.37	1.00		
C−H−C	0	28.5	6.00		
H−H−C	0	0	6.00		
H−H−H	0	27.9	6.00		

[a] This value leads to an equilibrium angle of 180−71.31=108.69° for the single-bond C−C−C valence angle (eq 8d).

TABLE 6: Torsion and Conjugation Parameters (V_2 and V_3 in kcal/mol) As Used in Equations 10a−c

torsion angle[a]	V_2	V_3	p_t
C−C−C−C	21.7	0.00	−2.42
C−C−C−H	30.5	0.58	−2.84
H−C−C−H	26.5	0.37	−2.33

[a] Torsion angles not defined in this table (i.e., C−H−C−C) are assigned torsion barrier energies of 0 kcal/mol.

equilibrium angle changes from around 109.47° for sp^3 hybridization (π-bond = 0) to 120° for sp^2 (π-bond = 1) to 180° for sp (π-bond = 2) based on the geometry of the central atom j and its neighbors. In addition to including the effects of π-bonds on the central atom j, eq 8d also takes into account the effects of over- and under-coordination in central atom j (Δ_j) on the equilibrium valency angle, including the influence of a lone electron pair. The functional form of eq 8d is designed to avoid singularities when SBO = 0 and SBO = 2. The angles in eqs 8a−d are in radians.

$$E_{val} = f_7(BO_{ij}) \cdot f_7(BO_{jk}) \cdot f_8(\Delta_j) \cdot \{k_a - k_a \exp[-k_b(\Theta_o - \Theta_{ijk})^2]\} \quad (8a)$$

$$f_7(BO_{ij}) = 1 - \exp(-\lambda_{11} \cdot BO_{ij}^{\lambda_{12}}) \quad (8b)$$

$$f_8(\Delta_j) = \frac{2 + \exp(-\lambda_{13} \cdot \Delta_j)}{1 + \exp(-\lambda_{13} \cdot \Delta_j) + \exp(p_{v,1} \cdot \Delta_j)} \cdot \left[\lambda_{14} - (\lambda_{14} - 1) \cdot \frac{2 + \exp(\lambda_{15} \cdot \Delta_j)}{1 + \exp(\lambda_{15} \cdot \Delta_j) + \exp(-p_{v,2} \cdot \Delta_j)}\right] \quad (8c)$$

$$SBO = \Delta_j - 2 \cdot \left\{1 - \exp\left[-5 \cdot \left(\frac{1}{2}\Delta_j\right)^{\lambda_{16}}\right]\right\} + \sum_{n=1}^{neighbors(j)} BO_{jn,\pi}$$

$$\Delta_{j,2} = \Delta_j \text{ if } \Delta_j < 0$$

$$\Delta_{j,2} = 0 \text{ if } \Delta_j \geq 0$$

$$SBO2 = 0 \text{ if } SBO \leq 0 \quad (8d)$$

$$SBO2 = SBO^{\lambda_{17}} \text{ if } 0 < SBO < 1$$

$$SBO2 = 2 - (2 - SBO)^{\lambda_{17}} \text{ if } 1 < SBO < 2$$

$$SBO2 = 2 \text{ if } SBO > 2$$

$$\Theta_0 = \pi - \Theta_{0,0} \cdot \{1 - \exp[-\lambda_{18} \cdot (2 - SBO2)]\}$$

To reproduce the stability of systems with two double bonds sharing an atom in a valency angle, like allene, an additional energy penalty, as described in eqs 9a and 9b, is imposed for

such systems. Equation 9b deals with the effects of over/undercoordination in central atom j on the penalty energy.

$$E_{pen} = \lambda_{19} \cdot f_9(\Delta_j) \cdot \exp[-\lambda_{20} \cdot (BO_{ij} - 2)^2] \cdot \exp[-\lambda_{20} \cdot (BO_{jk} - 2)^2] \quad (9a)$$

$$f_9(\Delta_j) = \frac{2 + \exp(-\lambda_{21} \cdot \Delta_j)}{1 + \exp(-\lambda_{21} \cdot \Delta_j) + \exp(\lambda_{22} \cdot \Delta_j)} \quad (9b)$$

2.5. Torsion Angles. Just as with angle terms we need to ensure that dependence of the energy of torsion angle ω_{ijkl} accounts properly for BO → 0 and for BO greater than 1. This is done by eqs 10a−c. The V_2-cosine term in eq 10a depends on the bond order of the central bond BO_{jk}. In torsion angles with a central double bond (BO_{jk} = 2) the V_2-term is at its maximum (about 30 kcal/mol, see Table 6). If BO_{jk} deviates from 2 the magnitude of the V_2-term rapidly diminishes. The valence-angle-dependent term $\sin(\Theta_{ijk}) \cdot \sin(\Theta_{jkl})$ in eq 10a ensures that the torsion energy contribution disappears when either of the two valence angles (Θ_{ijk} or Θ_{jkl}) approaches π.

$$E_{tors} = f_{10}(BO_{ij}, BO_{jk}, BO_{kl}) \cdot \sin\Theta_{ijk} \cdot \sin\Theta_{jkl}$$
$$\left[\frac{1}{2}V_2 \cdot \exp\{p_t(BO_{jk} - 3 + f_{11}(\Delta_j,\Delta_k))^2\} \cdot (1 - \cos 2\omega_{ijkl}) + \frac{1}{2}V_3 \cdot (1 + \cos 3\omega_{ijkl})\right] \quad (10a)$$

$$f_{10}(BO_{ij}, BO_{jk}, BO_{kl}) = [1 - \exp(-\lambda_{23} \cdot BO_{ij})] \cdot [1 - \exp(-\lambda_{23} \cdot BO_{jk})] \cdot [1 - \exp(-\lambda_{23} \cdot BO_{kl})] \quad (10b)$$

$$f_{11}(\Delta_j, \Delta_k) = \frac{2 + \exp[-\lambda_{24} \cdot (\Delta_j + \Delta_k)]}{1 + \exp[-\lambda_{24} \cdot (\Delta_j + \Delta_k)] + \exp[\lambda_{25} \cdot (\Delta_j + \Delta_k)]} \quad (10c)$$

To avoid excessive torsion contributions in systems containing two attached over-coordinated sp^3-carbon atoms, like an ethane molecule in which the central C−C bond length is reduced from its equilibrium value of about 1.52 Å to 1.35 Å, we include eq 10c, which reduces the influence of BO_{jk} on the V_2-term in eq 10a when atoms j and k are over-coordinated [$\Delta_j > 0$, $\Delta_k > 0$]. Equation 10b describes the smooth disappearance of the torsion energy contribution when one of the bonds in the torsion angle dissociates.

2.6. Conjugated Systems. Equations 11a and 11b describe the contribution of conjugation effects to the molecular energy. A maximum contribution of conjugation energy is obtained when successive bonds have bond-order values of 1.5 as in benzene and other aromatics.

$$E_{conj} = f_{12}(BO_{ij}, BO_{jk}, BO_{kl}) \cdot \lambda_{26} \cdot [1 + (\cos^2 \omega_{ijkl} - 1) \cdot \sin\Theta_{ijk} \cdot \sin\Theta_{jkl}] \quad (11a)$$

$$f_{12}(BO_{ij}, BO_{jk}, BO_{kl}) = \exp\left[-\lambda_{27} \cdot \left(BO_{ij} - 1\frac{1}{2}\right)^2\right] \cdot \exp\left[-\lambda_{27} \cdot \left(BO_{ij} - 1\frac{1}{2}\right)^2\right] \cdot \exp\left[-\lambda_{27} \cdot \left(BO_{kl} - 1\frac{1}{2}\right)^2\right] \quad (11b)$$

2.7. Nonbonded van der Waals Interactions. In addition to valence interactions which depend on overlap, there are repulsive interactions at short interatomic distances due to Pauli principle orthogonalization and attraction energies at long distances due to dispersion. These interactions, comprised of
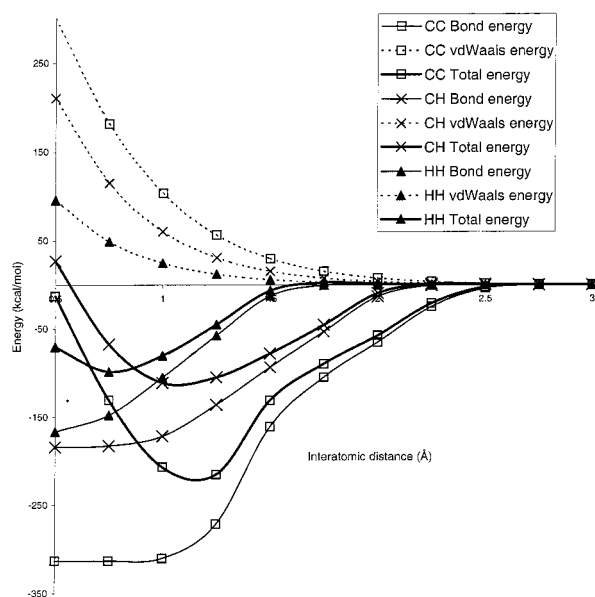
Figure 3. Interatomic distance dependency of the carbon−carbon, carbon−hydrogen, and hydrogen−hydrogen bond- and van der Waals-energy terms of diatomic C−C, C−H, and H−H systems. Energy contributions from Coulomb interactions and energy effects related to under and overcoordination are ignored in the total energy curve.

van der Waals and Coulomb forces, are included for *all* atom pairs, thus avoiding awkward alterations in the energy description during bond dissociation. In this respect, ReaxFF is similar in spirit to the central valence force fields that were used earlier in vibrational spectoscropy. To account for the van der Waals interactions we use a distance-corrected Morse-potential (eqs 12a,b). By including a shielded interaction (eq 12b), excessively high repulsions between bonded atoms (1−2 interactions) and atoms sharing a valence angle (1−3 interactions) are avoided. Figure 3 shows how the bond energies, derived from eq 5, combine with the van der Waals interactions for diatomic C−C, C−H, and H−H systems to give a dissociation energy curve.

$$E_{vdWaals} = D_{ij} \cdot \left\{ \exp\left[\alpha_{ij} \cdot \left(1 - \frac{f_{13}(r_{ij})}{r_{vdW}} \right) \right] - 2 \cdot \right.$$
$$\left. \exp\left[\frac{1}{2} \cdot \alpha_{ij} \cdot \left(1 - \frac{f_{13}(r_{ij})}{r_{vdW}} \right) \right] \right\} \quad (12a)$$

$$f_{13}(r_{ij}) = \left[r_{ij}^{\lambda_{29}} + \left(\frac{1}{\lambda_w} \right)^{\lambda_{28}} \right]^{1/\lambda_{28}} \quad (12b)$$

2.8. Coulomb Interactions. As with the van der Waals interactions, Coulomb interactions are taken into account between *all* atom pairs. To adjust for orbital overlap between atoms at close distances a shielded Coulomb potential is used.

$$E_{Coulomb} = C \cdot \frac{q_i \cdot q_j}{[r_{ij}^3 + (1/\gamma_{ij})^3]^{1/3}} \quad (13)$$

Atomic charges are calculated using the Electron Equilibration Method (EEM) approach.[20−21] The EEM charge derivation method is similar to the QEq scheme;[6] the only differences, apart from parameter definitions, are that EEM does not use an iterative scheme for hydrogen charges (as in QEq) and that QEq uses a more rigorous Slater orbital approach to account for charge overlap. However, the γ_{ij} in eq 13 can be optimized to reproduce the QEq orbital overlap correction. The initial values for the EEM-parameters (χ, η, and γ, Table 2) were taken from

Njo et al.,[22] but these parameters were allowed to change during the FF optimization procedure. Intraatomic contributions of atomic charges, to account for the energy required to polarize the atoms, are taken into account in the energy scheme,[23] thus allowing a straightforward expansion of the force field for ionic compounds.

With the EEM-parameter values from Table 2, ReaxFF assigns a charge of −0.113 to the carbon atoms in cyclohexane and charges of +0.050 and +0.063 to the equatorial and axial hydrogens, respectively. A Mulliken distribution, from a DFT calculation with the 6-31G**-basis set, results in charges of −0.174, +0.0859, and 0.0876 to the cyclohexane carbon, equatorial and axial hydrogens while the QEq method[6] gets a −0.24, +0.104, +0.137 charge distribution.

2.9. Force Field Optimization Procedure. The FF was optimized using a successive one-parameter search technique as described by van Duin et al.[24] In general, our aim was to reproduce heats of formation to within 4.0 kcal/mol, bond lengths to within 0.01 Å, and bond angles to within 2° of their literature values. To use the QC data in the FF optimization procedure, structures relating to these data were added to the FF training set. All molecules used in the heat of formation and geometry data comparisons were continuously energy minimized during the FF optimization while the structures relating to the QC data were kept fixed or were optimized with appropriate bond length or torsion angle restraints.

3. Results

3.1. Non-Conjugated Systems. *3.1.1. Energy and Geometry Reproduction.* Figure 4a and Table 7 show how well the ReaxFF reproduces the heat of formation for nonconjugated closed shell molecules. The heat of formation predictions for ReaxFF are compared with those of the semiempirical MOPAC-method,
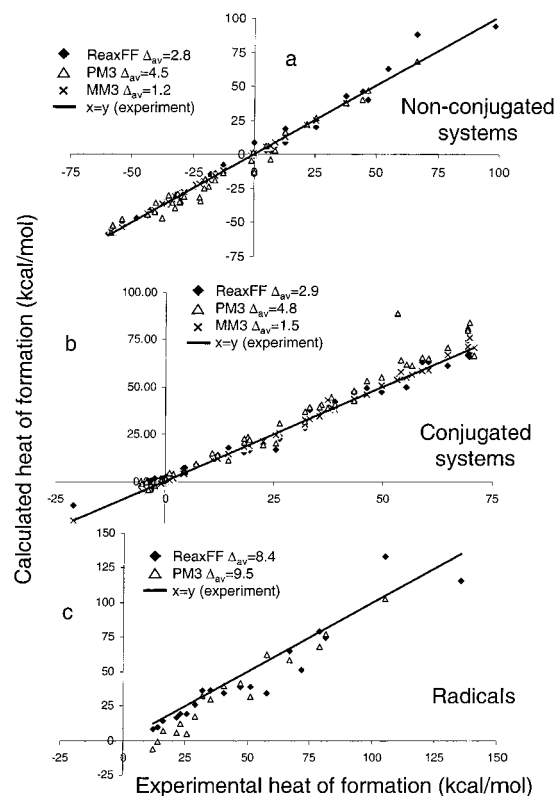

Figure 4. Comparison of calculated heats of formation with experimental data for nonconjugated (a), conjugated (b), and radical systems (c).

ReaxFF: A Reactive Force Field for Hydrocarbons

J. Phys. Chem. A, Vol. 105, No. 41, 2001 **9401**

TABLE 7: Heat of Formation (kcal/mol) from ReaxFF for Non-conjugated Systems

| compound	H_f(calc)	H_f(exp)[a]-POP	diff
cyclohexane	−30.65	−29.49	−1.16
ethane	−18.33	−20.02	1.69
isobutane	−30.62	−32.07	1.45
neopentane	−40.91	−40.18	−0.73
anti-*n*-butane	−29.69	−30.20[b]	0.31
ethylene	8.75	12.55	−3.80
propene	2.64	4.78	−2.14
allene	40.23	46.40[c]	−6.17
hydrogen	8.85	0.00	8.85
cyclopentane	−17.59	−18.45	0.86
trans-decaline	−45.14	−43.52	−1.62
cis-decaline	−41.13	−40.45	−0.68
cyclobutene	42.54	37.50	5.04
cyclopentene	6.35	8.56[d]	−2.21
cyclohexene	−2.57	−1.20	−1.37
norbornane	−8.00	−12.42	4.42
norbornene	20.67	21.52	−0.85
ethyne	63.06	54.50	8.56
propyne	46.43	44.20	2.23
cyclobutane	2.89	6.80	−3.91
cyclopropane	18.82	12.70	6.12
protoadamantane	−20.38	−20.54[e]	0.16
cis-hydrindane	−30.11	−30.41	0.30
perhydroquinacene	−21.40	−22.00	0.60
1,1-dimethylcyclopentane	−31.80	−33.33	1.53
2,2,3,3-tetramethylbutane	−49.56	−53.65	4.09
gauche-butene	−2.31	−0.50	−1.81
cyclopropene	88.35	66.23	22.12
cycloheptane	−27.99	−28.44[f]	0.45
cyclooctane	−28.51	−30.12[g]	1.61
cyclononane	−30.76	−32.26[h]	1.50
cyclodecane	−36.62	−37.56[I]	0.94
bicyclo[2.2.2]octane	−23.80	−23.68	−0.12
cis-bicyclo[3.3.0]octane	−21.77	−22.20	0.43
bicyclo[3.3.1]nonane	−31.32	−30.50	−0.82
trans-bicyclo[3.3.0]octane	−14.06	−15.91	1.85
di-*tert*-butylmethane	−55.13	−57.60	2.47
diamantane	−37.30	−34.87[e]	−2.43
tst-perhydroanthracene	−58.12	−58.21	0.09
adiene	19.87	25.24	−5.37
carbene	93.84	98.00	−4.16
methane	−14.25	−17.80	3.55

[a] Experimental heats of formation were taken from Pedley et al.[25] unless noted otherwise. [b] POP = −0.20 kcal/mol. [c] ref 26. [d] ref 27. [e] ref 28. [f] POP = −0.21 kcal/mol. [g] POP = −0.36 kcal/mol. [h] POP = −0.52 kcal/mol. [i] POP = −0.68 kcal/mol.

using the PM3-parameters[39] and with those of the nonreactive MM3 force field. Heats of formation data were calculated from the total system energy, as determined from eq 1, by adding the terms described in eq 14. POP in eq 14 reflects the contribution of high-energy conformations, defined as the difference in heat of formation between the most stable conformation and the mixture of conformations. These high-energy conformation contributions, which are primarily significant for the larger (C_{6+}) monocyclic saturated ring system in the training set, are also listed in Table 7. I_C and I_H in eq 14 are the heat increments for the carbon and hydrogen atoms, respectively, as given in Table 2. n_C and n_H are the number of carbon and hydrogen atoms in the molecule. $4RT$ is added to account for translation, rotation, and pV-work in nonlinear polyatomic molecules. The values for the heat increments were determined by calculating the system energies of the compounds in the force field training set, addition of the POP and $4RT$-contribution and subsequent optimization of I_C and I_H to minimize the difference between calculated and literature heats of formation. As a result, the heat increments values bear no direct physical meaning, as, apart from the heats of formation

TABLE 8: Geometry Predictions from ReaxFF (bond lengths in Å, angles in degrees) for Non-Conjugated Systems

compound	bond/angle[j]	calcd	expt
ethane[a]	a	1.555	1.53
	b	1.1198	1.10
	ab	110.6	110
	bb′	108.3	107
ethylene[b]	a	1.312	1.337
	b	1.117	1.08
	ab	121.0	121.8
	bb′	118.0	116.4
ethyne[c]	a	1.241	1.202
	b	1.104	1.06
hydrogen[c]	a	0.78	0.7414
cyclohexane[d]	a	1.551	1.54
	b	1.121	1.10
	aa′	111.2	111.0
	bb′	103.7	107.0
cyclopentene[e]	a	1.324	1.348
	b	1.552	1.52
	c	1.564	1.55
	ab	111.9	112.8
	bc	103.1	103.3
cyclohexene[f]	a	1.343	1.34
	b	1.546	1.50
	c	1.561	1.53
norbornane[g]	ab	90.9	93.9
norbornene[h]	ab	90.1	95.3
	bc	101.1	96.1
2,2,3,3-tetramethylbutane[i]	a	1.553	1.54
	b	1.569	1.58

[a] ref 20. [b] ref 30. [c] ref 31. [d] ref 32. [e] refs 33−34. [f] ref 35. [g] ref 36. [h] ref 37. [i] ref 38. [j] See Figure 24 for bond and angle definitions.
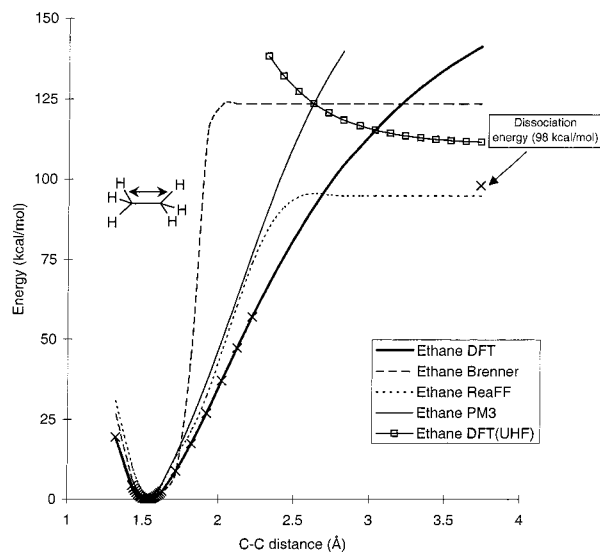
Figure 5. Ethane C−C bond dissociation. Crosses indicate the data used in the force field parametrization.

of the elements, they also contain corrections for vibrational and zero-point energy.

$$\Delta H_f = E_{system} + 4RT + POP + n_C I_C + n_H I_H \quad (14)$$

Table 8 shows the ReaxFF geometry data reproduction for nonconjugated molecules.

3.1.2. Reproduction of Quantum Chemical Data. Figures 5−7 show the carbon−carbon dissociation energies for ethane, ethylene, and ethyne as obtained from DFT calculations, the Brenner FF, PM3, and ReaxFF. The DFT calculations were performed at the B3LYP-level using the 6-31G** basis set, which includes Generalized Gradient Corrections and exact
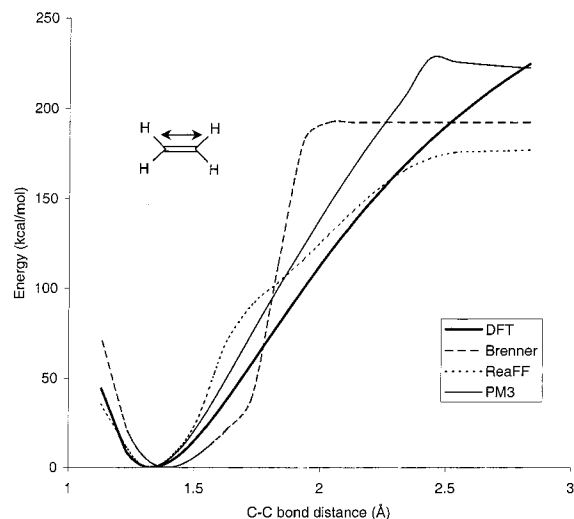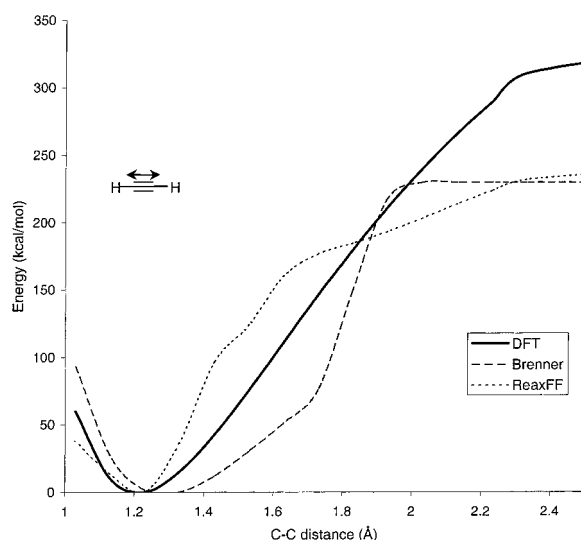
Figure 6. Ethylene C−C bond dissociation.

Figure 7. Ethyne C−C bond dissociation.

Figure 8. Propane C−H dissociation.

Figure 9. Hydrogen H−H bond dissociation.

Figure 10. Energy curve for a bridging methyl group.

Exchange energies. All these DFT bond dissociation calculations were performed using a restricted Hartree−Fock method on singlet spin systems. These restricted calculations are reliable when the bond lengths are close to their equilibrium values but tend to overestimate the bond energies at longer bond distances. For this reason, only the DFT data with C−C distances smaller than 1.5 times the equilibrium bond distance were used in the force field optimization procedure (see Figure 5 for an example). To demonstrate the overestimation of the bond dissociation energies by restricted singlet-state Hartree−Fock DFT calculations, data from an unrestricted Hartree−Fock calculation on the triplet spin systems have been added to the ethane dissociation curve in Figure 5. At C−C distances > 3.0 Å the energy from the unrestricted calculations become lower than those from the restricted calculations, reflecting a more proper sp^3-sp^3 dissociation energy.

Figure 8 shows the DFT, Brenner, PM3, and ReaxFF energies for methyl C−H dissociation in propane. Figure 9 compares the DFT and ReaxFF energies for a dissociating H_2 molecule. Figures 10 and 11 show the DFT, Brenner, PM3, and ReaxFF energies for systems containing a bridging methylene and a bridging hydrogen between two methyl groups, respectively. Figure 12 shows the DFT, ReaxFF, and PM3 energies of a hydrogen exchange between methyl and hydrogen radicals. Figures 13 and 14 compare the Brenner, PM3, and ReaxFF
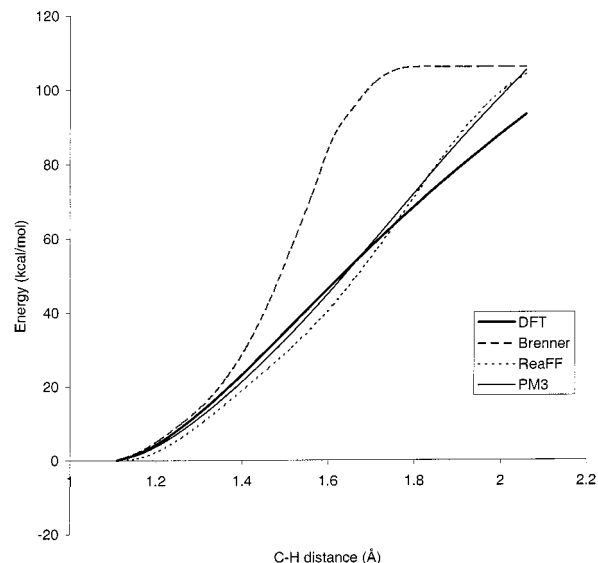
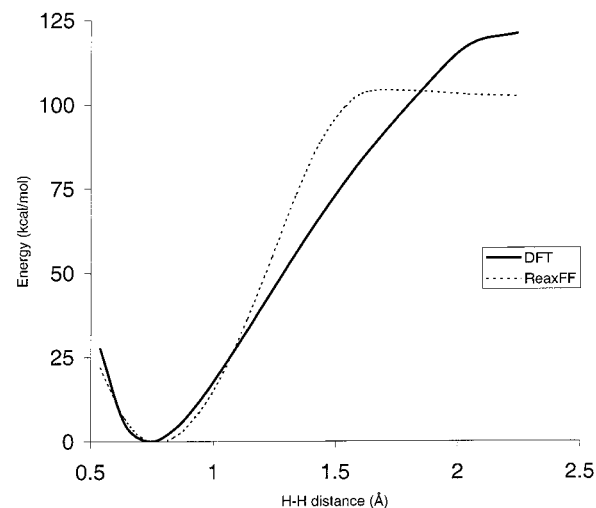reproduction of DFT data on the rotational barriers in ethylene and 2-butene, respectively. Figure 15 compares ReaxFF, PM3, and DFT energy data for an expanding adamantane molecule
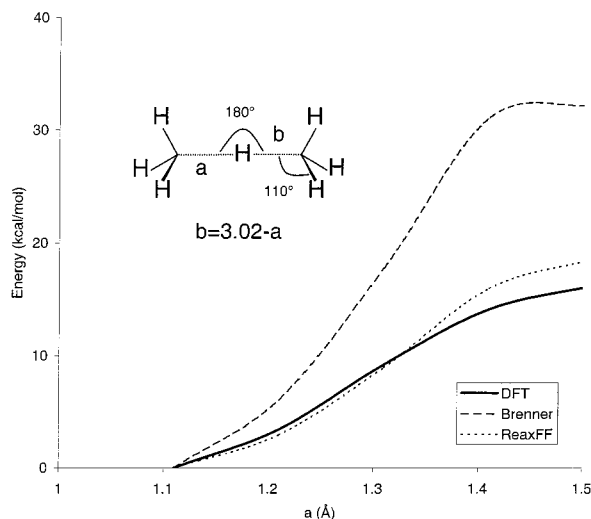
ReaxFF: A Reactive Force Field for Hydrocarbons

J. Phys. Chem. A, Vol. 105, No. 41, 2001 **9403**

Figure 11. Energy curve for a bridging hydrogen between two methyl radicals.
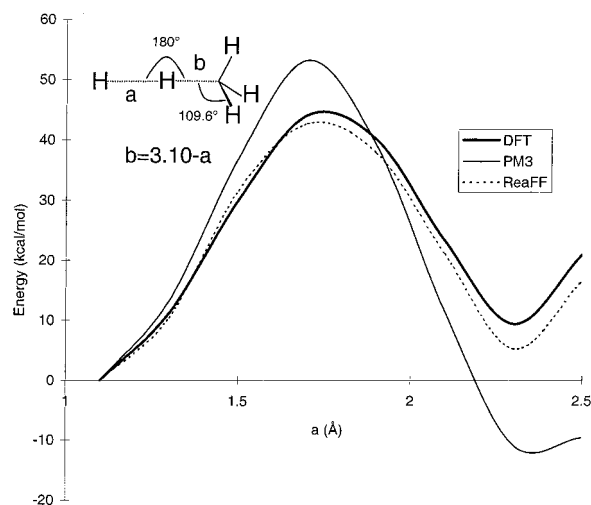
Figure 12. Energy curve for a bridging hydrogen between a methyl and a hydrogen radical.

Figure 13. Energy barrier for the rotation around the central C=C bond in ethylene.
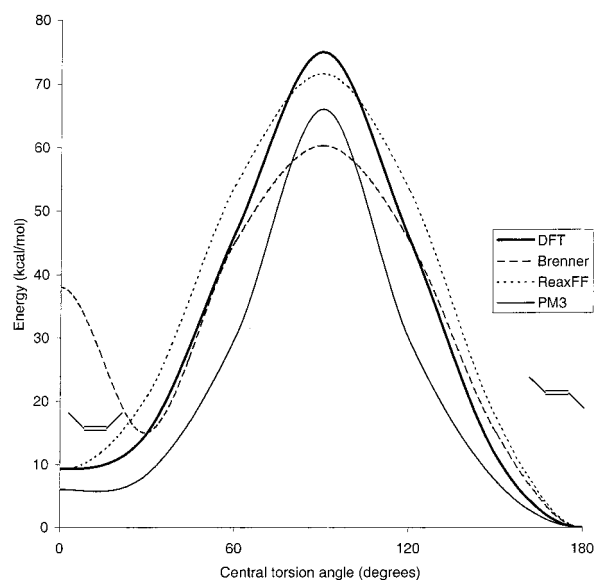
Figure 14. Energy barrier for the rotation around the central C=C bond in 2-butene.

(with fixed C−H distances). Figure 16 compares the DFT, PM3, ReaxFF, and Brenner energy data for a system of two approaching methane molecules. In all these cases, ReaxFF matches the DFT curves much better than the Brenner potential.

To optimize the ReaxFF hydrogen−hydrogen potential the data calculated by Liu for the linear H_3 case[40] were added to the training set. Liu found an energy barrier for the hydrogen exchange reaction of 9.8 kcal/mol ($r_{ab} = r_{bc} = 0.9294$ Å at the transition state). ReaxFF calculates an energy barrier of 10.6 kcal/mol for this reaction. DFT, Brenner, and PM3 calculate energy barriers of 6.1 kcal/mol, 10.0 kcal/mol, and −7.9 kcal/mol, respectively. In addition to the Liu data, some energy values for the linear H_3 case with very short hydrogen−hydrogen distances ($r_{ab} = r_{bc} = 0.635$ Å, $r_{ab} = 0.635$ Å; $r_{bc} = 0.741$ Å, and $r_{ab} = r_{bc} = 0.741$ Å) as calculated by Boothroyd et al.[41] were also used to optimize the hydrogen potential in ReaxFF. Figure 17 shows the influence of C−C−C valence angle bending on the stability of propane, propene, and propyne molecules, demonstrating that ReaxFF predicts proper equilibrium angles for sp³, sp2, and sp systems. Figure 18a shows that ReaxFF can also describe the influence of bond dissociation on valence angles by obtaining a smooth transition from H−C−H angles of around 108° in ethane to 120° in the methyl radicals resulting from C−C bond dissociation. The effects of
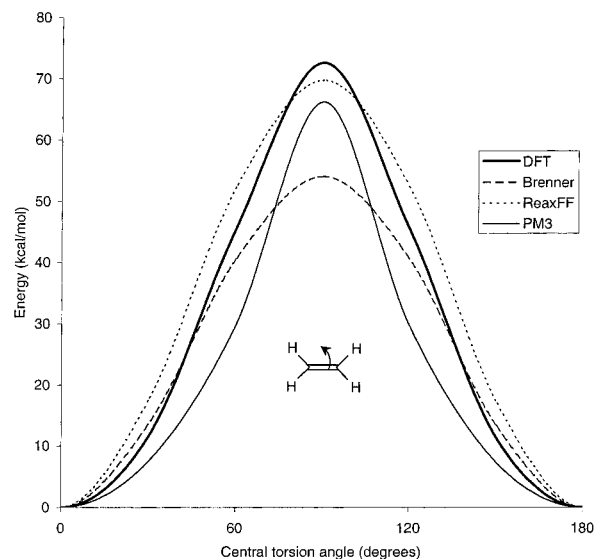
bond dissociation on torsion energy is demonstrated in Figure 18b, which shows the differences in energy between a staggered and the eclipsed conformation of ethane as a function of C−C bond distance. Both in Figure 18a and 18b the ReaxFF trajectories differ in shape from the DFT curve. However, ReaxFF reproduces the DFT data for both the nondissociated as well as the completely dissociated systems and describes a smooth trajectory between these systems.

3.2. Conjugated Systems. *3.2.1. Energy and Geometry Reproduction.* Figure 4b and Table 9 show the ReaxFF reproduction of experimental heat of formation data, compared with heat of formation data calculated using the PM3 and MM3-methods. Table 10 compares ReaxFF and experimental geometry data for conjugated closed-shell molecules.

3.2.2. Reproduction of Quantum Chemical Data. To optimize the conjugation parameters in eqs 10a and 10b, DFT data for the rotational barrier around the central C−C bond in 1,3-butadiene and DFT data concerning the rearrangement of benzene to cyclohexatriene were added to the training set. Figure 19 compares the performance of ReaxFF and PM3 to the DFT
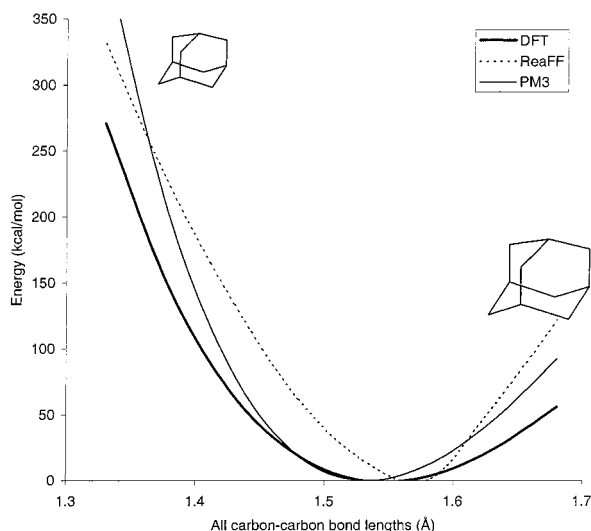
Figure 15. Energy curve for an dilating adamantane (uniform expansion of C−C bonds).
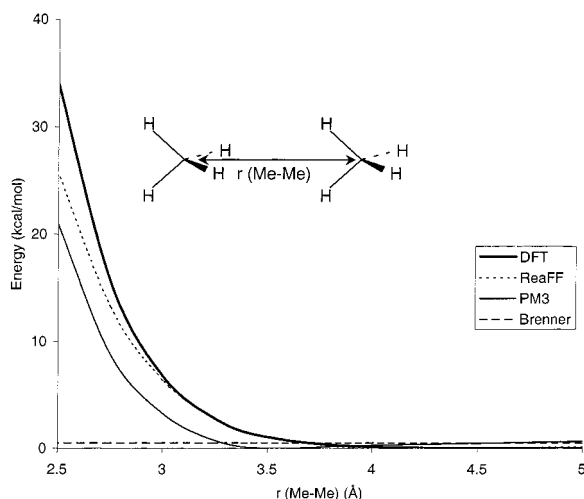

Figure 16. Energy curve for van der Waals repulsion between two methane molecules.

data for the butadiene rotational barrier. ReaxFF is significantly better here than PM3. Figure 20 shows the DFT, Brenner, PM3, and ReaxFF data for the rearrangement of benzene to cyclo-hexatriene. While ReaxFF is significantly better than Brenner, it is somewhat less accurate than PM3.

3.3. Radicals. *3.3.1. Energy Reproduction.* Figure 4c and Table 11 show the reproduction of experimental data on radical heats of formation by both the ReaxFF force field and PM3.

3.3.2. Reproduction of Quantum Chemical Data. Figures 21 and 22 compare the performance of ReaxFF to quantumchemical data on dissociation pathways of *n*-butylbenzyl radical and a 2-nonyl radical, respectively. Figure 23 shows the GVB and ReaxFF curves for the α, *β*, and *γ*-dissociation of *n*-butylben-zene. In contrast to the data in Figures 5−16 and 19−20, which were obtained from single point calculations (fixed geometries), the curves in Figures 16−18 were obtained by constraining the distance between the dissociating atoms and minimizing the energy of the rest of the molecular structures, thus allowing bond orders and geometries to adjust themselves to the changes in coordination.

3.4. Conformation Energy. Table 12 shows the ReaxFF reproduction of experimental data on differences in energy between various molecular conformations.
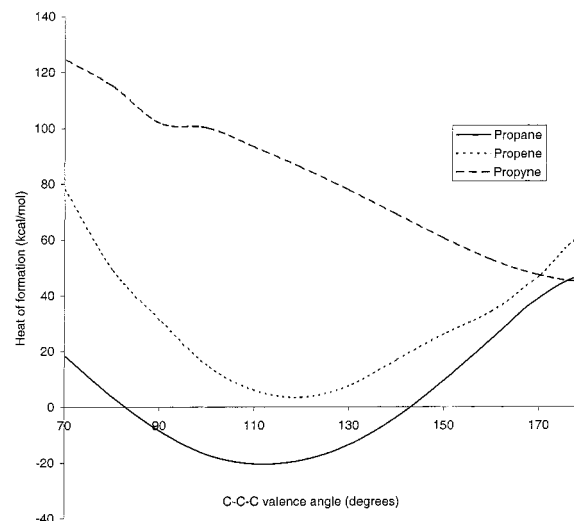

Figure 17. ReaxFF energy effects of C−C−C valence angle bending in propane, propene, and propyne. A valence angle restraint was used to force the C−C−C angles, the rest of the molecular geometry was energy minimized.
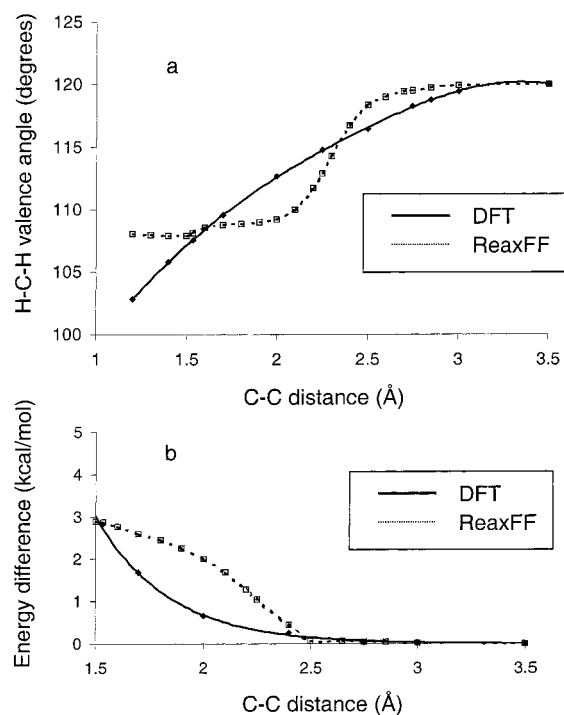

Figure 18. Effects of the dissociation of the C−C bond in ethane on (a) the H−C−H valence angle and (b) the energy difference between an eclipsed and staggered ethane molecule. Both in (a) and (b), a distance restraint was used to force the C−C bond to dissociate, the rest of the molecular geometry was energy minimized.

3.5. Crystals. Table 13 shows the ReaxFF reproduction of crystal data on graphite, diamond, buckyball, and cyclohexane. ReaxFF predicts the packing energy of 1.35 kcal/mol/°C difference between a single sheet of graphite and a graphite crystal, which is in good agreement with the literature value of 1.3 kcal/mol °C.[68]

4. Discussion

Compared to other computational methods (MM3, PM3, Brenner, and DFT) ReaxFF provides a very simple and parameter-efficient method (93 parameters) for describing hydrocarbon systems. This efficiency and transparency provides

ReaxFF: A Reactive Force Field for Hydrocarbons

J. Phys. Chem. A, Vol. 105, No. 41, 2001 **9405**

TABLE 9: Heat of Formation (in kcal/mol) Predicted with ReaxFF for Conjugated Systems

compound	H_f(calcd)	H_f(exp)[a]	diff
trans-1,3-butadiene	22.65	26.29	−3.64
benzene	21.07	19.00	2.07
naphthalene	34.39	35.92	−1.53
cyclohexadiene	16.98	25.38	−8.40
cyclopentadiene	30.13	32.10	−1.97
dimethylfulvene	28.20	32.12	−3.92
anthracene	49.77	55.19	−5.42
twist-biphenyl	47.06	43.36	3.70
trans-stilbene	56.70	56.43	0.27
cis-stilbene	63.49	60.30	3.19
azulene	67.16	69.10[b]	−1.94
chrysene	61.38	64.48	−3.10
hexamethylbenzene	−12.78	−20.75	7.97
2,3-dimethylbutadiene	12.91	10.78	2.13
trans-1,3-pentadiene	15.41	18.19[b]	−2.78
cis-1,3-pentadiene	16.51	19.46	−2.95
pyrene	54.46	53.94	0.52
4,5-dimethylphenanthrene	49.40	46.27	3.13
1,3,5-cycloheptatriene	47.32	43.24	4.08
1,3-cycloheptadiene	20.93	22.54	−1.61
cyclooctatetraene (boat)	70.72	70.72	0.00
styrene	35.55	35.35	0.20
indene	42.29	39.05	3.24
isoprene	18.04	18.04	0.00
tetracene	66.33	69.65	−3.32
3,4-benzophenanthrene	68.03	69.60	−1.57
phenanthrene	47.34	49.59	−2.25
toluene	14.10	12.05	2.05
o-xylene	7.44	4.57	2.87
m-xylene	7.19	4.13	3.06
p-xylene	6.99	4.30	2.69
1,2,3-trimethylbenzene	1.61	−2.27	3.88
1,2,4-trimethylbenzene	0.44	−3.30	3.74
1,3,5-trimethylbenzene	0.22	−3.80	4.02
ethylbenzene	8.83	7.15	1.68
1-methyl-2-ethylbenzene	2.45	0.31	2.14
1-methyl-3-ethylbenzene	1.88	−0.43	2.31
1-methyl-4-ethylbenzene	1.72	−0.76	2.48
propylbenzene	2.69	1.89	0.80
iso-propylbenzene	3.32	0.96	2.36
butylbenzene	−3.11	−3.13	0.02
tert-butylbenzene	−2.62	−5.40	2.78
iso-butylbenzene	−3.50	−5.14	1.64
sec-butylbenzene	−1.46	−4.16	2.70
indane	17.71	14.51	3.20
acenaphthene	41.72	37.28	4.44
fluoranthene	79.62	69.07	10.55
1,1-diphenylethylene	63.14	58.70	4.44
1,1-diphenylethane	37.81	33.15	4.66
9,10-dihydroanthracene	41.48	38.17	3.31
5,12-dihydrotetracene	54.91	53.11	1.80

[a] Experimental heats of formation were taken from Pedley et al.[25] unless noted otherwise. [b] ref 28.

an advantage for extending this method to non-hydrocarbon systems. Furthermore, apart from the Brenner potential, ReaxFF is the only method that can realistically be applied for predicting reactivity on larger molecules or multimolecular systems, as MM3 has not been designed to describe bond dissociation and QC-methods such as DFT and even semiempirical methods such as PM3 are too time-consuming. As Figure 25 demonstrates, with ReaxFF, nanoseconds MD simulations of reactions in C_{100+} systems become an option.

As the results indicate, ReaxFF has, on the whole, a larger deviation from the literature heat of formation data than MM3 (Figure 4). This is largely due to the fact that MM3 uses a number of empirical corrections, like heat of formation increments for specific structural features (e.g., tertiary and quaternary carbons) and special parameters for five-, four-, and three-

TABLE 10: Geometry Predicted from ReaxFF (bond lengths in Å, angles in degrees) for Conjugated Systems

compound	bond/angle[j]	calcd	expt
benzene[a]	a	1.400	1.399
	b	1.111	1.10
naphthalene[b]	a	1.435	1.417
	b	1.371	1.381
	c	1.437	1.422
	d	1.460	1.412
cyclohexadiene[c]	a	1.332	1.350
	b	1.509	1.468
	c	1.522	1.523
	d	1.581	1.534
cyclopentadiene[d]	a	1.333	1.342
	b	1.535	1.469
	c	1.553	1.510
trans-isoprene[e]	a	1.330	1.340
	b	1.535	1.463
	c	1.316	1.340
	d	1.555	1.512
azulene[f]	a	1.409	1.399
	b	1.426	1.418
	c	1.420	1.383
	d	1.383	1.406
	e	1.408	1.403
	f	1.518	1.501
1,3,5,7-cyclooctatetraene[g]	a	1.345	1.340
	b	1.551	1.475
phenanthrene[h]	a	1.430	1.394
	b	1.375	1.401
	c	1.441	1.409
	d	1.454	1.420
	e	1.451	1.465
	f	1.368	1.350
	g	1.443	1.453
	h	1.434	1.423
	i	1.375	1.386
4,5-dimethylphenanthrene[i]	1−6	2.932	2.976
	2−3−4	126.2	125.1
	1−2−3	123.6	124.0
	2−3−4−5	27.6	31.5
	1−2...5−6	62.7	67.4

[a] ref 42. [b] ref 43. [c] ref 44. [d] ref 45. [e] ref 46. [f] ref 47. [g] ref 48. [h] ref 49. [i] ref 50. [j] See Figure 24 for bond and angle definitions.
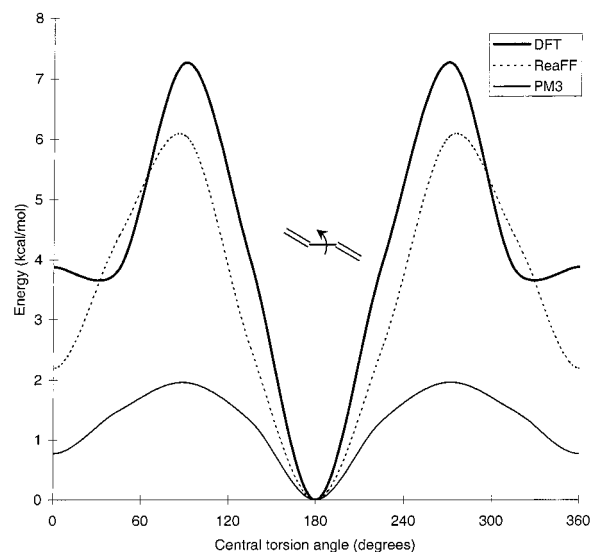
Figure 19. Energy barrier for the rotation around the central C−C bond in 1,3-butadiene.

membered rings. Such methods are difficult to implement in a reactive description, as a smooth transformation from one structural feature to another is not automatic and user intervention is required. For this reason, ReaxFF uses just two heat
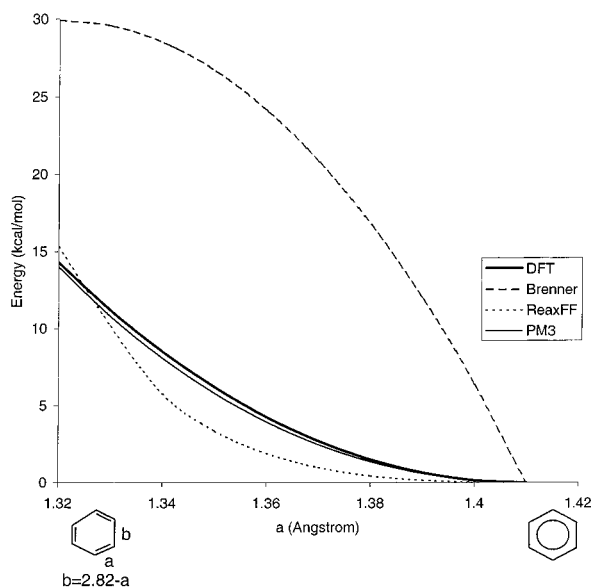
Figure 20. Energy curve for the rearrangement of cyclohexatriene to benzene.

TABLE 11: Heat of Formation (kcal/mol) Predicted from ReaxFF for Radicals

compound	H_f(calcd)	H_f(expt)[a]	diff
methyl radical	36.10	34.99	1.11
1-isobutyl radical	13.92	16.11	−2.19
tert-butyl radical	7.92	12.30	−4.38
1-propyl radical	19.28	23.30	−4.02
2-propyl radical	16.95	21.50	−4.55
2-propenyl radical	34.46	40.80	−6.34
2-propynyl radical	74.27	81.41	−7.14
ethyl radical	25.77	28.90	−3.13
ethenyl radical	51.42	71.70	−20.28
ethynyl radical	115.35	135.30	−19.95
cyclopropyl radical	64.64	66.90	−2.26
cyclobutyl radical	38.98	51.20	−12.22
cyclopentyl radical	18.94	25.60	−6.66
cyclohexyl radical	9.49	13.91	−4.42
cyclopropenyl radical	133.12	105.09	28.03
cyclopentadienyl radical	34.29	57.91	−23.62
cyclohexadienyl radical	38.71	47.08	−8.37
1-norbornyl radical	36.27	32.00	4.27
benzyl radical	78.96	78.90	0.06

[a] Experimental heats of formation were taken from the *Handbook of Chemistry and Physics*, 77th ed.[31]

parameters (one for carbon and one for hydrogen) and uses the same parameter set irrespective of the structural environment. Given these restrictions, reproduction of heat of formation data is very encouraging, showing that ReaxFF gives a good energy description for both strained and unstrained hydrocarbon systems. The ReaxFF heats of formation compare well with those of PM3, but this comparison might be biased since ReaxFF has been parametrized using these data. When comparing the heats of formation of radicals, ReaxFF successfully reproduces the extra stability of more highly coordinated radical centers (e.g., the ReaxFF calculates 1-isobutyl radical to be less stable than the *tert*-butyl radical and 1-propyl radical to be less stable than 2-propyl radical, see Table 11). On the whole, ReaxFF tends to overestimate the stability of radicals.

ReaxFF provides a good reproduction of the geometrical features of nonconjugated systems (Table 8). Especially of note is the fact that ReaxFF reproduces the shortening of sp^3-sp^2 bonds relative to sp^3-sp^3 bonds (see, for example, the cyclopentene and cyclohexene data in Table 8) since, in contrast to nonreactive hydrocarbon force fields such as MM3, special
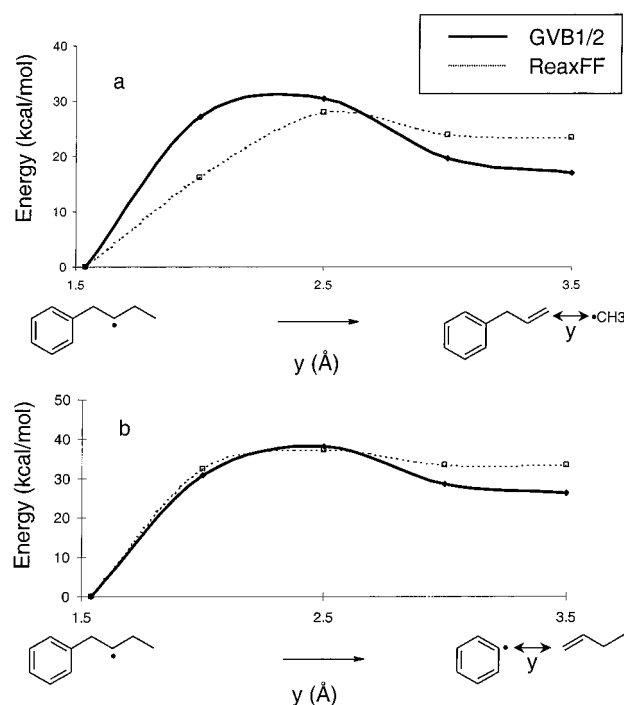

Figure 21. Energy curves for the dissociation reactions of an *n*-butylbenzene radical to propenebenzene and methyl radical (a) and to benzene radical and 1-butene (b).
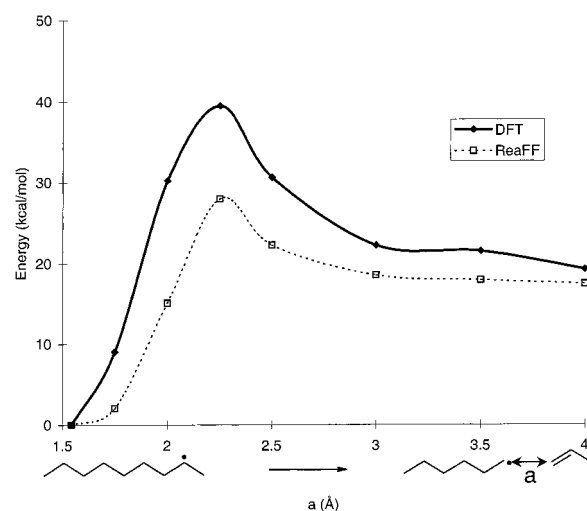

Figure 22. Energy curve for the dissociation reaction of 2-nonyl radical to 1-hexyl radical and propene.

parameters for sp^3-sp^2 bonds have not been included in ReaxFF. The deviation for conjugated systems between the ReaxFF and literature geometries is in general larger than for the nonconjugated systems (Table 10). However, in general ReaxFF manages to identify the variations in bond lengths between the bonds in conjugated systems, indicating the ReaxFF should be able to simulate the reactivity of conjugated systems.

The comparison between ReaxFF and experimental data on energy differences between molecular conformations (Table 12) shows that ReaxFF is able to provide a realistic simulation of the conformational distribution in hydrocarbon molecules. This, combined with the previously discussed heat of formation and geometry results and the good reproduction of crystal data (Table 13) shows that the ReaxFF functions well as a nonreactive force field. Obviously, the real potential of ReaxFF lies in its ability to simulate the reactivity of hydrocarbons. When using the DFT data on bond dissociation as a yardstick, ReaxFF seems to

ReaxFF: A Reactive Force Field for Hydrocarbons

J. Phys. Chem. A, Vol. 105, No. 41, 2001 **9407**

TABLE 12: Energy Differences ($E_2 - E_1$) in kcal/mol between Molecular Conformations Calculated by ReaxFF

conformation 1	conformation 2	ΔE (calcd)	ΔE (expt)
anti-*n*-butane[a]	gauche-*n*-butane	1.2	0.8
anti-*n*-butane[a]	eclipsed-*n*-butane	5.2	4.6
ethane (staggered)[b]	ethane (eclipsed)	2.8	2.9
2,2,3,3-tetramethylbutane (stag.)[c]	2,2,3,3-tetramethylbutane (ecl.)	3.6 (ΔE)	10.1 ($\Delta\Delta G$)
cyclohexane (chair)[d]	cyclohexane (twist-boat)	5.6	5.5
biphenyl (twist)[e]	biphenyl (90°)	3.2	1.0
biphenyl (twist)[e]	biphenyl (planar)	0.6	2.0
isoprene (trans)[f]	isoprene (90°)	3.9	5.78
styrene (planar)[g]	styrene (90°)	4.3	3.90
1,3,5-cycloheptatriene (boat)[h]	1,3,5-cycloheptatriene (planar)	7.5	5.8
1,3,5,7-cyclooctatetraene (boat)[i]	1,3,5,7-cyclooctatetraene (planar)	16.1	13.7

[a] refs 51−53. [b] ref 54. [c] ref 55. [d] ref 56. [e] ref 57. [f] ref 58. [g] ref 59. [h] ref 60. [i] ref 61.

TABLE 13: Crystal Data Predicted with ReaxFF (cell parameters in Å and degrees, energies in kcal/mol)

crystal		a	B	C	α	β	γ	energy
graphite (288 atoms)[a]	expt	7.58	8.75	6.67	90	90	90	0.0 (ΔH_f)
	calcd	7.50	8.67	6.60	90	90	90	0.69
diamond (256 atoms)[b]	expt	3.58	3.58	3.58	90	90	90	0.8 (ΔH_f)
	calcd	3.61	3.61	3.61	90	90	90	1.22
buckyball[c]	expt	13.6	14.2	14.2	90	90	90	44.1 (ΔH_{sub})
	calcd	13.73	14.36	14.43	90	90	90	38.3
cyclohexane[d]	expt	11.2	6.4	8.2	90	109	90	11.1 (ΔH_{sub})
	calcd	11.84	6.59	8.52	90	109	90	12.6

[a] refs 62−63. [b] ref 31. [c] ref 64−65. [d] ref 66−67.
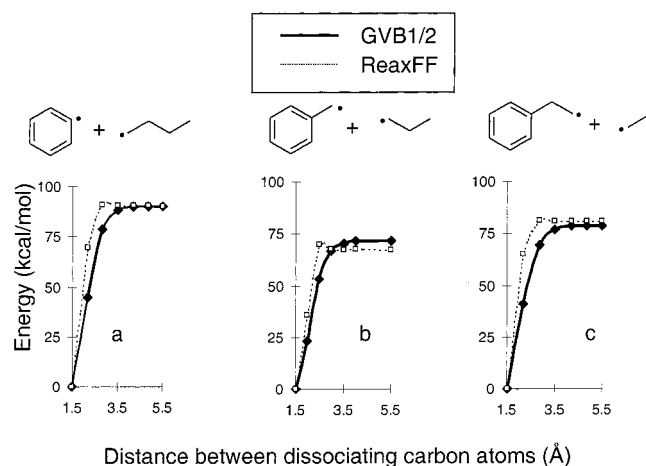
Figure 23. Energy curves for the α- (a), β- (b), and (c) γ-dissociation of the side-chain in *n*-butylbenzene.

provide a smoother and more realistic description of bond dissociation compared to the Brenner potential and results quite similar to the PM3 method. The ethane, ethylene, ethyne C−C, and propane C−H dissociation curves (Figures 5−7) show a kink in the Brenner potential energy between 1.6 and 1.8 Å. ReaxFF does not suffer from this anomaly. The problems with the Brenner potential become more apparent when comparing the energy curves for the bridging methyl and hydrogen (Figures 10 and 11) where the Brenner potential greatly overestimates the energy barrier for these exchange reactions, while both ReaxFF and PM3 reproduce the DFT data very well. The Brenner potential also seems to have problems with very short H- - -H contacts, as evident from the 2-butene rotational barrier (Figure 14). Since the methyl groups were not allowed to relax during the rotation around the central double bond a very close H- - -H contact of 1.39 Å develops when the two methyl groups eclipse (central torsion angle 0°). As Figure 14 indicates, both ReaxFF and PM3 are capable of dealing with this. The Brenner potential, however, greatly overestimates the repulsion between the two nearby hydrogens, which is surprising since the Brenner potential does not contain nonbonded van der Waals and

Coulomb-type interactions. This lack of nonbonded interactions in the Brenner potential becomes evident in Figure 16, in which both ReaxFF and PM3 give good reproductions of the DFT repulsion energy between two approaching methane molecules, while the Brenner potential fails to register any energy effect from this. Figure 20 shows that ReaxFF reproduces the DFT energy data for the cyclohexatriene-to-benzene transformation quite well (although not as well as PM3), while the Brenner energy curve deviates strongly, indicating that ReaxFF provides a more realistic description of the conversion from conjugated to nonconjugated systems. Further confirmation of the applicability of ReaxFF to conjugated systems is obtained from the comparison of the DFT data regarding the rotational barrier in 1,3-butadiene to the ReaxFF-data. Finally, the good reproduction of the quantum-chemical reaction curves for bond dissociations in *n*-butylbenzene and 2-nonyl radical (Figures 21−23) show that ReaxFF cannot only simulate simple dissociation reactions but can also be applied for more elaborate reaction mechanisms in which bond dissociation is accompanied by changes in bond orders and major molecular rearrangements.

As mentioned earlier, an important application for ReaxFF will be the simulation of the reactive behavior of relatively large (containing over 100 carbon atoms) hydrocarbon systems, especially systems in which the reactive centers cannot be identified a priori. In identifying applications one should keep in mind that ReaxFF provides an empirical, rather than a fundamental, description of hydrocarbon stability and chemical bond dissociation. For this reason, ReaxFF will not be able to simulate every aspect of hydrocarbon reactivity. As an example, when simulating the ring opening of cyclobutene to butadiene, ReaxFF is unlikely to reproduce the preference of a disrotatory over a conrotatory ring opening, as this preference is based on orbital symmetries not included in ReaxFF. However, being able to describe the intrinsic stability of the various bonds in cyclobutene, ReaxFF will be able to give a good prediction on the overall reaction rate for this ring opening. The potential and limitations of ReaxFF can be further demonstrated by comparing its performance in reproducing the reaction barriers for 4+2 and 2+2 Diels−Alder reactions. For the allowed 4+2 reaction
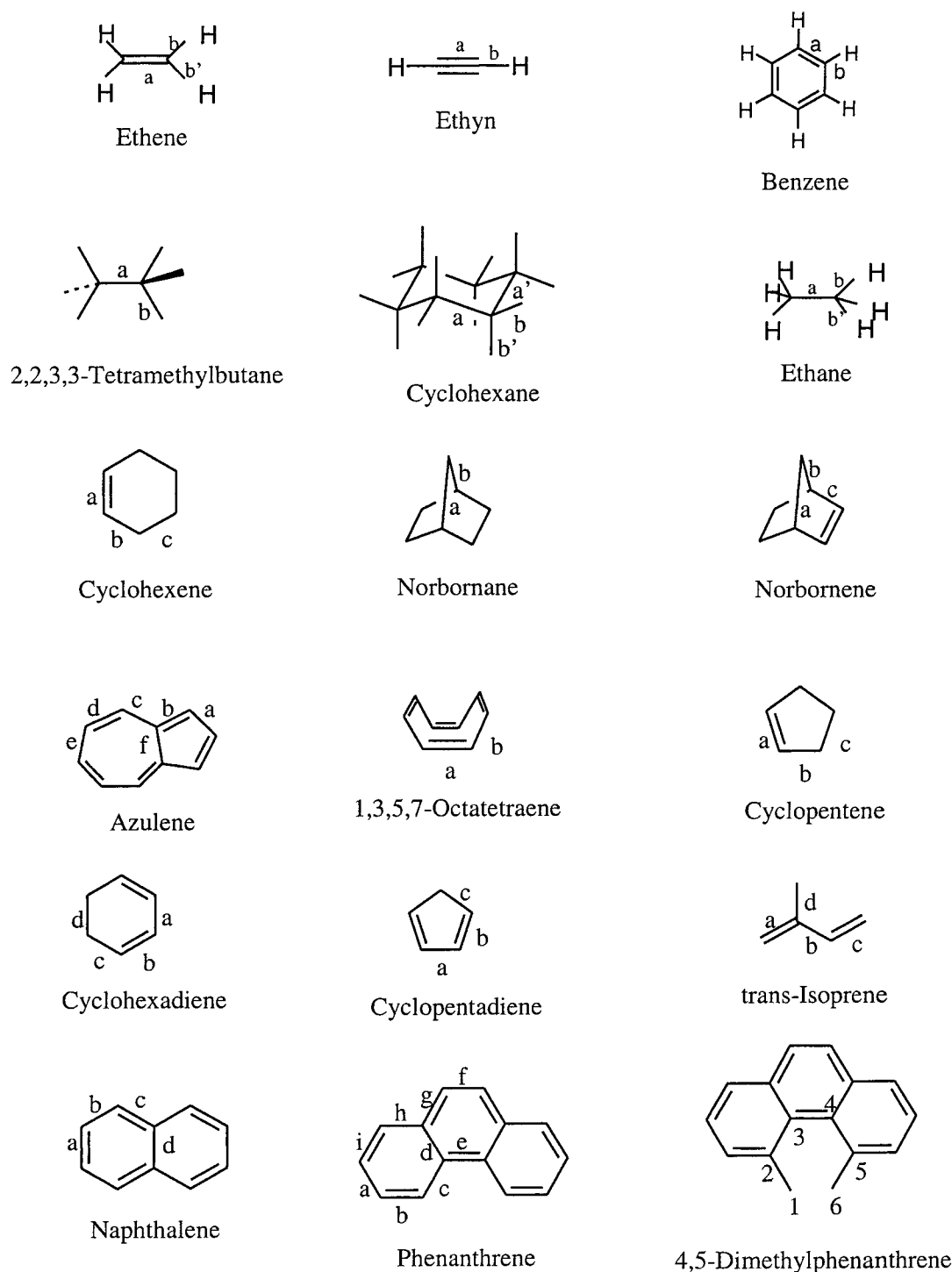
Figure 24. Bond and valence angle definitions.

of butadiene and ethylene to cyclohexene ReaxFF gives a good reproduction of the reaction barrier (ReaxFF: 33 kcal/mol; HF/6-31G**/MP4: 25 kcal/mol). However, for the 2+2 reaction of two ethylene molecules to cyclobutane ReaxFF fails to fully reproduce the increase in reaction barrier by allowing the forbidden planar approach pathway (ReaxFF: 39 kcal/mol; experimental barrier:[69] 62.5 kcal/mol). Keeping these limitations in mind ReaxFF provides a useful tool for studying hydrocarbon reactivity.

5. Conclusion

ReaxFF, a reactive force field, has been designed to describe the stability and geometry of nonconjugated, conjugated, and radical-containing compounds and, additionally, to describe the dissociation and formation of chemical bonds in hydrocarbon compounds. The results have been compared with an extensive set of literature heat of formation and geometry data on one hand and quantum chemical data on bond dissociation in various simple hydrocarbon molecules on the other hand. This comparison shows that ReaxFF can indeed reproduce the energies associated with the nonreactive and reactive behavior of these compounds.

Compared to the quantum-chemical or semiempirical methods currently used for simulating reactivity in hydrocarbon systems, ReaxFF provides a much faster method. Because of this, ReaxFF allows simulations on the formation and dissociation of chemical
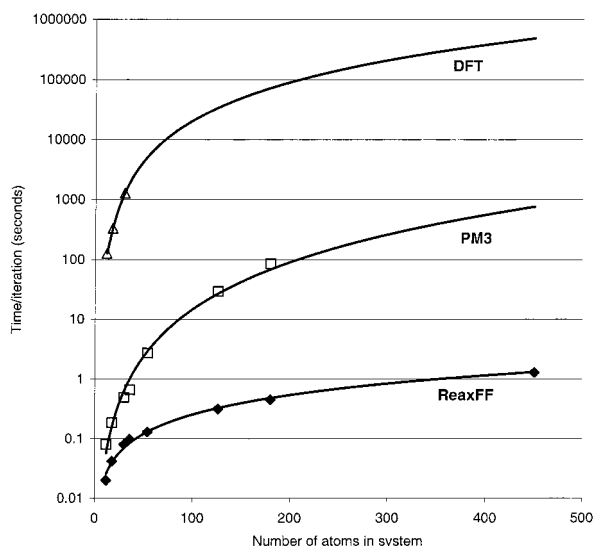
ReaxFF: A Reactive Force Field for Hydrocarbons

J. Phys. Chem. A, Vol. 105, No. 41, 2001 **9409**

Figure 25. Influence of molecular system size on computer time. Calculations were performed on single- and multimolecular aromatic systems using one processor of a Silicon Graphics Origin-computer (R10000 processor, 195 MHz).

bonds in relative large hydrocarbon systems (C_{100+}), thus opening up new possibilities for computational chemistry.

References and Notes

(1) Allinger, N. L.; Yuh, Y. H.; Lii, J.-H. *J. Am. Chem. Soc.* **1989**, *111*, 8551.
(2) Allinger, N. L.; Li, F.; Yan, L. *J. Comput. Chem.* **1990**, *11*, 848.
(3) Allinger, N. L.; Li, F.; Yan, L.; Tai, J. C. *J. Comput. Chem.* **1990**, *11*, 868.
(4) Mayo, S. L.; Olafson, B. D.; Goddard, W. A. *J. Phys. Chem.* **1990**, *94*, 8897.
(5) Rappé, A. K.; Casewit, C. J.; Colwell, K. S.; Goddard, W. A.; Skiff, W. M. *J. Am. Chem. Soc.* **1992**, *114*, 10024.
(6) Rappé, A. K.; Goddard, W. A. *J. Phys. Chem.* **1991**, *95*, 3358.
(7) Brenner, D. W. *Phys. Rev. B* **1990**, *42*, 9458.
(8) Che, J.; Cagin, T.; Goddard, W. A. *Nanotech.* **1999**, *10*, 263.
(9) Johnston, H. S.; Parr, C. *J. Am. Chem. Soc.* **1963**, *85*, 2544.
(10) Johnston, H. S. *Adv. Chem. Phys.* **1960**, *3*, 131.
(11) Pauling, L. *J. Am. Chem. Soc.* **1947**, *69*, 542.
(12) Sato, S. *J. Chem. Phys.* **1955**, *23*, 2465.
(13) Espinosa-Garcia, J. *J. Phys. Chem. A* **2001**, *105*, 134.
(14) Blowers, P.; Masel, R. I. *J. Phys. Chem. A* **1998**, *102*, 9957.
(15) Chandra, A. K.; Rao, V. S. *Chem. Phys.* **1995**, *200*, 387.
(16) Root, D. M.; Landis, C. M.; Cleveland, T. *J. Am. Chem. Soc.* **1993**, *115*, 4201.
(17) Cleveland, T.; Landis, C. M. *J. Am. Chem. Soc.* **1996**, *118*, 6020.
(18) Landis, C. M.; Cleveland, T.; Firman, T. K. *J. Am. Chem. Soc.* **1998**, *120*, 2641.
(19) Dennison, D. M. *Philos. Mag.* **1926**, *1*, 195.
(20) Mortier, W. J.; Ghosh, S. K.; Shankar, S. *J. Am. Chem. Soc.* **1986**, *108*, 4315.
(21) Janssens, G. O. A.; Baekelandt, B. G.; Toufar, H.; Mortier, W. J.; Schoonheydt, R. A. *J. Phys. Chem.* **1995**, *99*, 3251.
(22) Njo, S. L.; Fan, J.; van de Graaf, B. *J. Mol. Catal. A* **1998**, *134*, 79.
(23) Smirnov, K. S.; van de Graaf, B. *J. Chem. Soc., Faraday Trans.* **1996**, *92*, 2469.
(24) van Duin, A. C. T.; Baas, J. M. A.; van de Graaf, B. *J. Chem. Soc., Faraday Trans.* **1994**, *90*, 2881.
(25) Pedley, J. B.; Naylor, D.; Kirby, S. P. *Thermochemical Data of Organic Compounds*; Chapman and Hall: London, 1986.
(26) Curtiss, L. A.; Raghavachari, K.; Redfern, P. C.; Pople, J. A. *J. Chem. Phys.* **1997**, *106*, 1063.
(27) Benson, S. W.; Cruickshank, F. R.; Golden, D. M.; Haugen, G. R.; O'Neal, H. E.; Rodgers, A. S.; Shaw, R.; Walsh, R. *Chem. Rev.* **1969**, *69*, 279.
(28) Cox, J. D.; Pilcher, G. *Thermochemistry of Organic and Orga-nomethallic Compounds*; Academic Press: London, 1970.
(29) Kuchitsu, K. *J. Chem. Phys.* **1968**, *49*, 4456.
(30) Bartell, L. S.; Roth E. A.; Hollowell, C. D.; Kuchitsu, K.; Young, Y. E. *J. Chem. Phys.* **1965**, *42*, 2683.
(31) *Handbook of Chemistry and Physics, 77th ed.*; CRC Press: New York, 1996.
(32) Bastiansen, O.; Fernholt, L.; Seip, H. M. *J. Mol. Struct.* **1973**, *18*, 163.
(33) Saebø, S.; Cordell, F. R.; Boggs, J. E. *J. Mol. Struct.* **1983**, *104*, 221.
(34) Davis, M. I.; Muecke, T. W. *J. Phys. Chem.* **1970**, *74*, 1104.
(35) Chiang, J. F.; Bauer, S. H. *J. Am. Chem. Soc.* **1969**, *91*, 1898.
(36) Allinger, N. L.; Geise, H. J.; Pyckhout, W.; Paquette, L. A.; Galluci, J. C. *J. Am. Chem. Soc.* **1989**, *111*, 1106.
(37) Chaing, J. F.; Chiang, R.; Lu, K. C. *J. Mol. Struct.* **1977**, *41*, 67.
(38) Bartell, L. S.; Boates, T. L. *J. Mol. Struct.* **1976**, *32*, 379.
(39) Stewart, J. J. P. *J. Comput. Chem.* **1989**, *10*, 209.
(40) Liu, B. *J. Chem. Phys.* **1973**, *58*, 1925.
(41) Boothroyd, A. I.; Keogh, W. J.; Martin, P. G.; Peterson, M. R. *J. Chem. Phys.* **1991**, *95*, 4343.
(42) Tamagawa, K.; Iijima, T.; Kimura, M. *J. Mol. Struct.* **1976**, *30*, 243.
(43) Ketkar, S. N.; Fink, M. *J. Mol. Struct.* **1981**, *77*, 139.
(44) Oberhammer, H.; Bauer, S. H. *J. Am. Chem. Soc.* **1969**, *91*, 10.
(45) Hagen, K.; Traetteberg, M. *Acta Chem. Scand.* **1972**, *26*, 3643.
(46) Traetteberg, M.; Paulen, G.; Cyvin, S. J.; Panchenko, Y. N.; Mochalov, V. I. *J. Mol. Struct.* **1984**, *116*, 141.
(47) Bastiansen, O.; Derissen, J. L. *Acta Chem. Scand.* **1966**, *20*, 1319.
(48) Traetteberg, M. *Acta Chem. Scand.* **1966**, *20*, 1724.
(49) Kay, M. I.; Okaya, Y.; Cox, D. E. *Acta Crystallogr.* **1971**, *B27*, 26.
(50) Armstrong, R. N.; Ammon, H. L.; Darnow, J. N. *J. Am. Chem. Soc.* **1987**, *109*, 2077.
(51) Heenan, R. K.; Bartell, L. S. *J. Chem. Phys.* **1983**, *78*, 1270.
(52) Wiberg, K. B.; Murcko, M. A. *J. Am. Chem. Soc.* **1988**, *110*, 8029.
(53) Compton, D. A. C.; Montero, S.; Murphy, W. F. *J. Phys. Chem.* **1980**, *84*, 3587.
(54) Hirota, E.; Endo, Y.; Saito, S.; Duncan, J. L. *J. Mol. Spectrosc.* **1981**, *89*, 285.
(55) Anderson, J. E.; Pearson, H. *J. Am. Chem. Soc.* **1975**, *97*, 764.
(56) Squillacote, M.; Sheridan, R. S.; Chapman, O. L.; Anet, F. A. L. *J. Am. Chem. Soc.* **1975**, *97*, 3244.
(57) Almenningen, A. J.; Bastiansen, O.; Fernholt, L.; Cyvin, B. N.; Cyvin, S. J.; Samdal, S. *J. Mol. Struct.* **1985**, *128*, 59.
(58) Panchenko, Y. N.; Pupyshev, V. I.; Abramenkov, A. V.; Traetteberg, M.; Cyvin, S. J. *J. Mol. Struct.* **1985**, *130*, 355.
(59) Almlof, J. E.; Isacsson, P. V.; Mjoberg, P. J.; Ralowski, M. *Chem. Phys. Lett.* **1974**, *26*, 215.
(60) Lambert, J. B.; Durham, L. J.; Lepoutere, P.; Roberts, J. D. *J. Am. Chem. Soc.* **1965**, *87*, 3896.
(61) Anet, F. A. L. *J. Am. Chem. Soc.* **1962**, *84*, 671.
(62) Bailey, A. C.; Yates, B. *J. Appl. Phys.* **1970**, *41*, 5088.
(63) Ganster, W. G.; Fritz, I. J. *J. Appl. Phys.* **1974**, *45*, 3309.
(64) Guo, Y.; Karasawa, N.; Goddard, W. A. *Nature* **1991**, *351*, 464.
(65) Pan, C.; Sampson, M. P.; Chai, Y.; Hauge, R. H.; Margrave, J. L. *J. Phys. Chem.* **1991**, *95*, 2944.
(66) Kahn, R.; Fourme, R.; André, D.; Renaud, M. *Acta Crystallogr. Sect. B* **1973**, *29*, 131.
(67) Kitaigorodsky, A. I. *Molecular Crystals and Molecules*; Academic Press: New York, 1979; p 335.
(68) Goddard, W. A.; Karasawa, N. Unpublished data.
(69) Genaux, C. T.; Kern, F.; Walters, W. D. *J. Am. Chem. Soc.* **1953**, *75*, 6196.